RESEARCH

High-performance graphene–PbS quantum dots hybrid photodetector with broadband response and long-time stability

Jiajin Zheng[1] · Wanchao Di[1] · Beibei Bao[1] · Jiaqi Lu[1] · Kehan Yu[1] · Wei Wei[1]

Abstract

In this work, a graphene photodetector hybrid with lead sulfide quantum dots (PbS QDs) is introduced, aiming to take both the advantages of broad-spectrum absorption of PbS QDs and ultrafast carrier mobility of graphene. Through coating the PbS QDs on the graphene, a hybrid photodetector was successfully fabricated, and the optical response of this device to the photo illumination was observed from 405 to 980 nm. The experimental results show that the photoresponsivity of the hybrid photodetector is 7.7×10^2 A·W^{-1}, 6.4×10^2 A·W^{-1}, 5.4×10^2 A·W^{-1} and 2×10^2 A·W^{-1} under 0.16 mW/cm^2 laser illumination of 405 nm, 515 nm, 650 nm and 980 nm, respectively. The maximum photoresponsivity of this device is 7.7×10^2 A·W^{-1} (8.93×10^9 Jones). The photoconductive gain is 3×10^7. Moreover, the device can maintain steady photoresponse for more than 250 s and 25 on/off switching cycles at least. It is believed that such a device fabricated by controllable graphene film and PbS QDs with long-time photoresponse stability in broadband spectrum will stimulate the development of novel graphene photodetectors.

1 Introduction

Graphene has promising potential in fabricating phototransistors and photodetectors owing to its unique electronic band structure with prominent optoelectronic and charge transport properties, such as mechanical strength and flexibility, air stability, heat and electrical conductivity, optical transparency, and high room temperature charge mobilities of 10^5 cm^2/V·s [1–4].

So far, the fabrication of graphene photodetectors still encounters certain complications and difficulties, especially the technical challenges in forming a large-area detector array. Though mechanical exfoliation of graphene is a relatively simple method, it still confronts limitations in terms of size, yield, and thickness control, and is unsuitable for industrialization [5]. In contrast, graphene based on chemical vapor deposition has become the alternative [6]. However, the inevitability of wrinkles and the transfer process-induced

✉ Jiajin Zheng
  zhengjj@njupt.edu.cn

  Kehan Yu
  kehanyu@njupt.edu.cn

1 College of Electronic and Optical Engineering,
  Nanjing University of Posts and Telecommunications,
  Nanjing 2100231, China

polymer residue often limit the performance and reliability of optoelectronic devices fabricated from CVD-grown graphene [7]. Therefore, research on the reliability of photodetectors based on large-area graphene film field effect transistor features a significant importance in the application of photodetection [8, 9].

Besides, pure graphene photodetector with low absorbance (optical absorbance of single sheet is about 2.3% at 550 nm [10]) has a huge negative influence for photodetection. Numerous approaches have been reported to improve the performance of graphene devices, including graphene-quantum dots hybrid detectors, a graphene semiconductor heterojunction [11], graphene p–n junction, etc. [11–13]. Graphene hybrid with quantum dots can ideally improve the photoresponsivity and strengthen the light absorption. High-quality PbS QDs have high molar absorption coefficients ($\approx 10^6$ M^{-1} cm^{-1}) [14] and can offer a wide range of bandgaps (0.6–1.6 eV) [15]. Moreover, the electronic properties of PbS QDs can be easily modified by surface ligand chemistry [16]. All these features promote PbS QDs as superior candidates for low-cost broad-spectrum photodetectors [17]. The hybrid structure comprising graphene and PbS QDs is atomically thin, forming a flexible and transparent device. Particularly, the fabrication of graphene–PbS QDs hybrid structure is a solution-based process, which additionally

possesses the merits of simplicity, inexpensiveness, and suitability for large-scale production [18].

In this paper, a hybrid photodetector, which consists of graphene–PbS QDs hybrid structures, is successfully fabricated and demonstrated to possess excellent electrical properties. Specifically, the graphene film is directly grown on the target substrate with no metal transfer by means of plasma-enhanced chemical vapor deposition (PECVD). Physical mask is used to sputter the electrode, which has a higher successful rate compared with the photolithography technology. As a result, our device displays a clear photoresponse to incident laser in the wavelength at least ranging from 405 to 980 nm. It can maintain the detection ability under laser radiation for more than 250 s (> 25 cycles); what is more, the photocurrent of each cycle keeps nearly the original shape.

2 Experimental details

A structural diagram of the graphene–PbS QDs hybrid photodetector is shown in Fig. 1a. The prepared device consists of multiple layers of, in the following order, p-doped silicon (Si, 450 ± 25 μm), silica (SiO_2, 300 nm), graphene films (1 ~ 4 layer), source and drain electrodes (Cu, 200 nm), and PbS quantum dots (QDs, 10.26 ± 0.1 nm). The graphene film is deposited on SiO_2/Si wafer by using the radio-frequency plasma-enhanced chemical vapor deposition (RF-PECVD) method [7]. During the growth process, a gasket should be put under the SiO_2/Si sheet, since the growth of graphene is in a 360-degree direction. Setting the RF plasma power, passing the mixed gas of CH_4 and H_2 to the reaction chamber, and adjusting the gas proportion and the power level, monolayer graphene films or few layers of graphene films will be obtained.

The PbS QDs are synthesized through a hot injection route [19]. Typically, 0.18 g PbO, 4 mL OA and 12 mL octadecene (ODE) were mixed and heated to 120 ℃ for 50 min under vacuum. Then 4 ml ODE of 0.0128 g S powder was quickly injected into the reaction flask and allowed to cool naturally. Finally, the PbS QDs with oil solubility

were precipitated and dispersed in cyclohexane to produce a 20 mg/mL solution. The PbS QDs have oil capacity, and the proportions of ligands and quantum dots are 38.7% and 61.3%, respectively. The Cu source/drain electrodes are deposited by direct-current sputtering with a thickness of 200 nm. The optical image of the photodetector is shown in Fig. 1b. The active channel width and length are 1000 μm and 30 μm, respectively. All of the active channels and source/drain electrodes are patterned using nickel shadow masks.

In the experiment, the Raman spectrum was measured with a Raman spectrometer (EZM-785-A2) with laser excitation at 532 nm (2.33 eV). The surface morphology of graphene was measured with field emission scanning electron microscopy (SEM, Hitachi S-4800). High-resolution transmission electron microscope (TEM) image was measured with field emission transmission electron microscope (Hitachi H-7000). The absorbing spectrum was measured with a UV–Vis–NIR spectrophotometer (PerkinElmer Lambda 950). Both the electrical and optoelectronic performance tests of the device were performed with a probe station using a Keithley 4200 A with a series of laser sources. All the measurements were performed at room temperature in air without any device encapsulation.

3 Results and discussion

The Raman spectra of different layers of graphene films on SiO_2 are shown in Fig. 2a. The ratio of the intensity of the 2D peak at ~2692 cm^{-1} to that of the G peak at ~1591 cm^{-1} for graphene is larger than 2, implying that a monolayer graphene film is obtained. Similarly, the four-layer result can be obtained as shown in Fig. 2a. The D peak reflects the degree of disorder in the crystal structure, so the weak D peak indicates the graphene fabricated by the PECVD method has little defects [20]. The representative SEM image of graphene surface is shown in Fig. 2b. The graphene film has a hexagonal shape. The graphene has a large area of 50 μm × 50 μm, which benefits from the advantage of the PECVD method. The TEM image of PbS QDs is exhibited in Fig. 2c and the SEM image of PbS QDs on Si/SiO_2 substrate is shown in Fig. 2d.

The SEM image of PbS QDs on Si/SiO_2 substrate is shown in Fig. 2e. It can be observed that the QDs are quite uniform and disperse well on the substrate. The optical absorption spectrum of PbS QDs in the UV and near-infrared (NIR) region is shown in Fig. 2f. It is obvious from this figure that the PbS QDs have absorption of UV light, and the absorbance decreases with the increase of wavelength. In particular, there is an obvious absorption peak at 1464 nm. Compared with the absorption spectrum of single-layer graphene shown in Fig. S1, PbS QDs have obvious
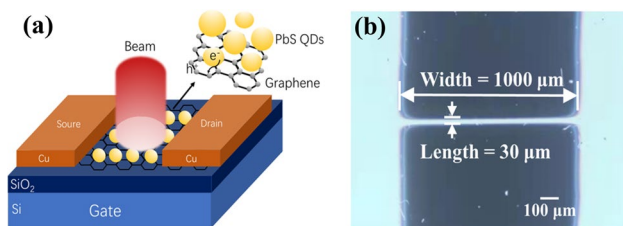
Fig. 1 a Schematic configuration of the graphene–PbS QDs hybrid photodetector. **b** The optical image of the photodetector

Fig. 2 **a** Raman spectrum of monolayer and four-layer graphene films on SiO$_2$. **b** SEM original images of graphene grown by PECVD on Si/SiO$_2$ substrate. **c** TEM image of PbS QDs. **d** SEM image of PbS QDs on Si/SiO$_2$ substrate. **e** The size distribution of PbS QDs. **f** The optical absorption spectrum of PbS QDs
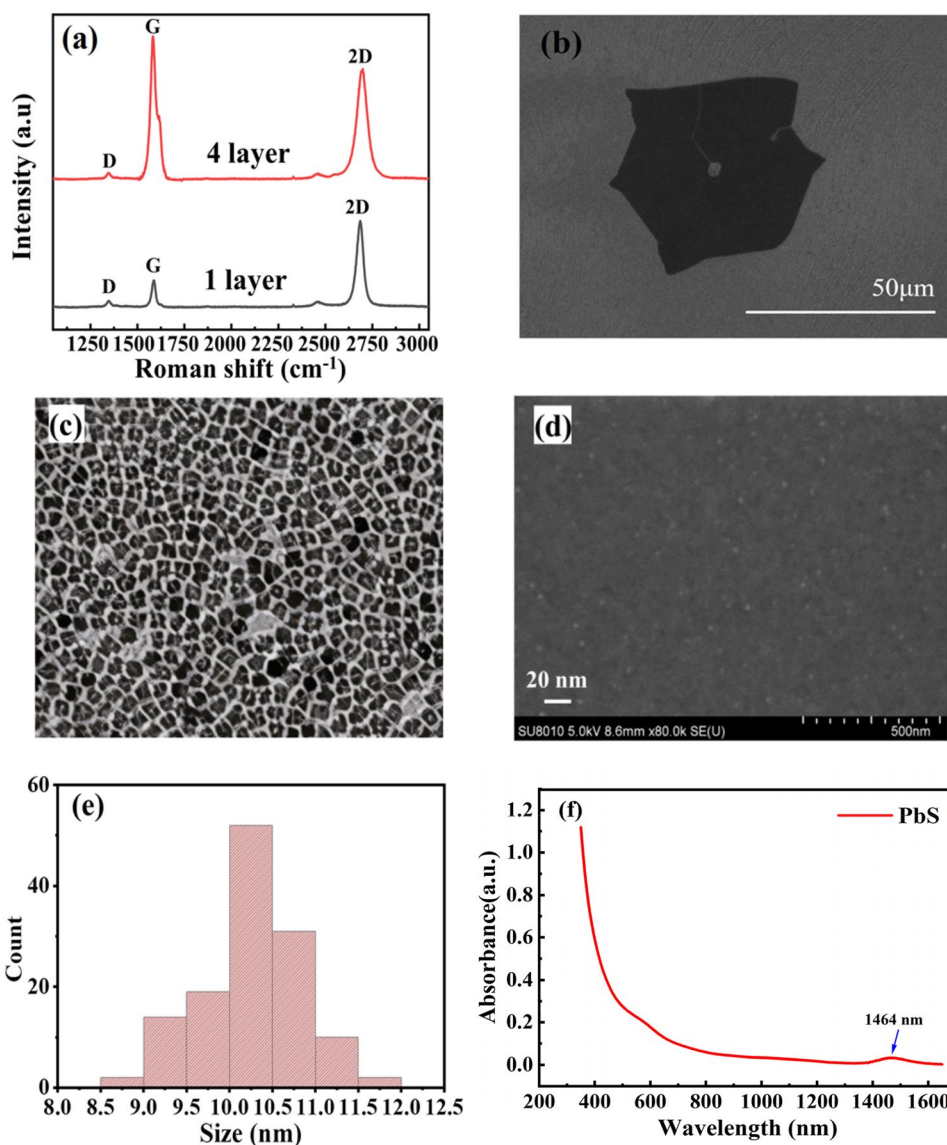
absorption enhancement from visible to near-infrared wave. At this point, graphene–PbS photodetector has the capability of broadband photodetection under the irradiation from the UV to NIR band.

Figure 3a shows the relationship curves between current Ids and voltage V_{ds} of drain and source when the gate voltage V_{gs} is 0 V. The two I_{ds}–V_{ds} curves represent the condition of the device with and without light illumination, respectively. The larger slope curve is measured under the light of 405 nm with an illumination power of 0.16 mW/cm^2. It can be clearly observed that the source and drain currents are in both cases proportional to the source and drain voltages, which indicates that the electrodes of the device make perfect Ohmic contact with the channel. Additionally, the proportional coefficient of the I_{ds}–V_{ds} curve increased and the curve became steeper when the device was exposed to the 405 nm laser, revealing that

the generation of photocurrent increases the total current under the same source–drain bias voltage, resulting in the change of the proportional coefficient of the I_{ds}–V_{ds} curve.

Figure 3b shows the transfer curve of the hybrid photodetector when the bias voltage of source and drain is 0.2 V. From this curve, the Dirac point shift from 3.7 to 5.3 V before and after the light illumination. Under dark condition, holes in PbS QDs are transferred to graphene leads to p-doping of graphene due to the built-in electric field formed by energy band mismatch. Under illumination, the PbS QDs absorb photon energy and generate electron–hole pairs. Electron–hole pairs are separated and photo-generated holes enter graphene, while photo-generated electrons remain in the PbS QDs, further inducing more photo-generated holes into graphene, which causes the Dirac point to continue moving to the right until the production and

Fig. 3 **a** Source–drain I_{ds}–V_{ds} curves of graphene–PbS QDs hybrid photodetector with and without light illumination (wavelength: 405 nm). **b** Transfer curves of graphene–PbS QDs hybrid photodetector before and after the light illumination, and the V_{ds} is 0.2 V. **c** The electronic band diagram of PbS QDs and graphene with light illumination. **d** Temporal photocurrent response at 405 nm. The rise time is 0.2213 s. The fall time is 0.6282 s
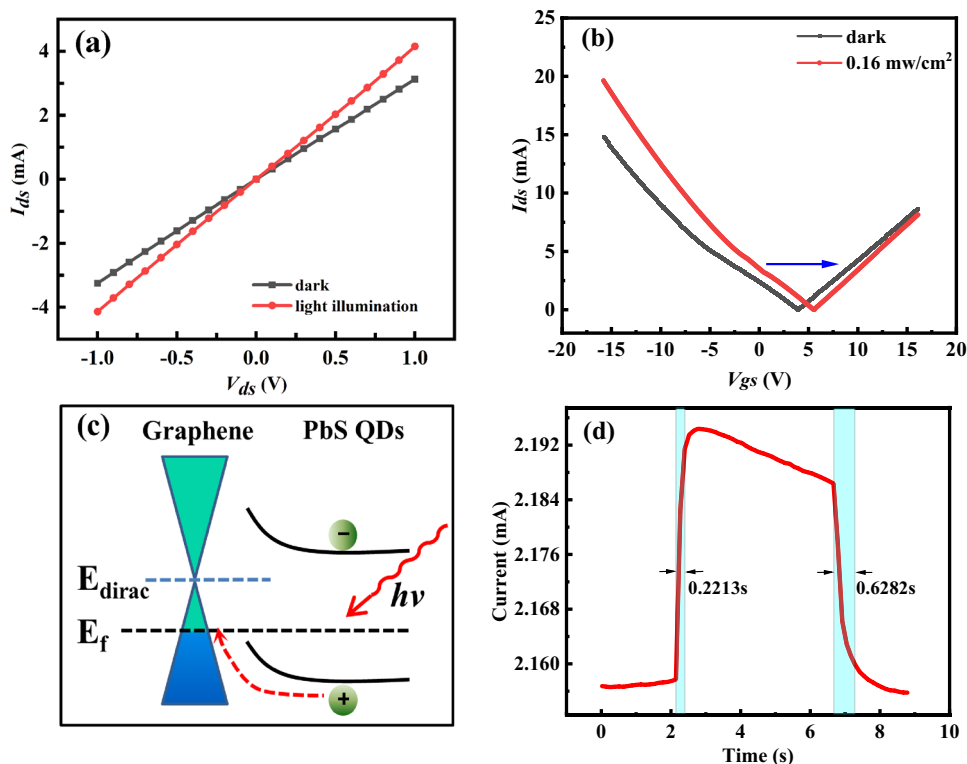
recombination rates in the system remain in balance. The energy band diagram is shown in Fig. 3c [21].

Furthermore, Fig. 3d shows the single period photo-generated current response curve of the graphene–PbS QDs hybrid photodetector under 405 nm laser illumination. The current results from the electron–hole pairs excited by the 405 nm illumination light with photon energy larger than the PbS QDs band gap. The current of the hybrid photo-detector rapidly increases when the 405 nm laser source is switched on at 2.1 s and decays after the laser source is switched off at 6.6 s. The photocurrent ($I_{ph} = I_{light} - I_{dark}$) can be approximately calculated as 0.037 mA, which is about 5 times to pure graphene photodetector as shown in Fig. S2. It is indicated that thin films of PbS QDs can greatly enhance the optical absorption and improve the photocurrent of the device. Furthermore, the rising time of the photocur-rent is 0.2213 s and the decay time of the photocurrent is 0.6282 s when the laser source is switched on and off. Since long oleic acid ligand was used without ligand exchange, the response speed of this device is slower than other PbS-graphene devices using short ligands, but it can fulfill some normal requirements.

To demonstrate the broadband spectral response char-acteristics of the hybrid photodetector, a series of lasers with different incident wavelengths were used to illuminate the graphene–PbS QDs hybrid photodetector. The results are shown in Fig. 4a–d measured under 405, 515, 650, and 980 nm laser illumination, respectively. It can be clearly

seen from these four species that the hybrid photodetector successfully features a clear photoresponse to incident laser in the wavelength range from 405 to 980 nm, exhibiting a broadband photoresponse characteristic. Furthermore, the hybrid photodetector also keeps a repeatable photocurrent and response speed for all illumination light after 6 on/off switching cycles, which indicates the excellent repro-ducibility and stability of the graphene–PbS QDs hybrid photodetector.

In addition to the broadband photodetection, the pho-toresponsivity also needs to be considered at different wavelengths. The photoresponsivity characteristics of the graphene–PbS QDs hybrid photodetector are measured at 1 V source–drain bias and zero gate voltage by illumi-nating the whole device at various wavelengths at room temperature. For rigorous comparison, laser sources at the visible (405 nm, 515 nm and 650 nm) and the NIR (980 nm) were set to the same power (0.16 mW/cm²) in the photoresponsivity measurements. The photocurrent (I_{ph}) depends on the current change before and after illumi-nations. According to Fig. 4a–d, According to Fig. 4a–d, we get the photocurrent spectrum of the device shown in Fig. 5a. It can be observed that the I_{ph} are 0.037 mA, 0.032 mA, 0.027 mA, and 0.01 mA, corresponding to the wavelength of 405 nm, 515 nm, 650 nm, and 980 nm, respectively. Apparently, the values of photocurrent vary greatly when under different incident lasers and the pho-tocurrent increases monotonically with the decreasing of

Fig. 4 Photoswitching characteristics of the graphene–PbS QDs hybrid photodetector under alternating dark and light illumination. The channel length was 30 μm, illumination power $P_i = 0.16$ mW/cm², $V_{ds} = 0.2$ V, $V_{gs} = 0$ V. **a** Wavelength = 405 nm. **b** Wavelength = 515 nm. **c** Wavelength = 650 nm. **d** Wavelength = 980 nm
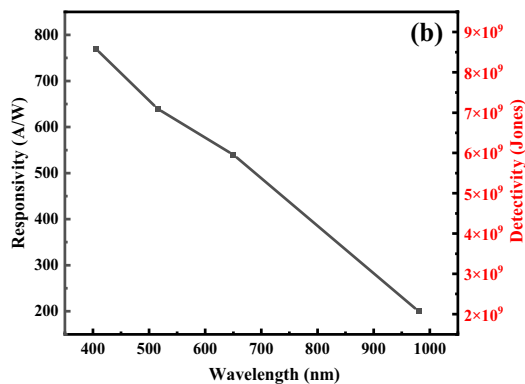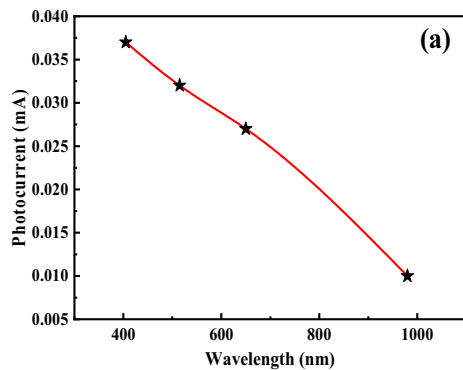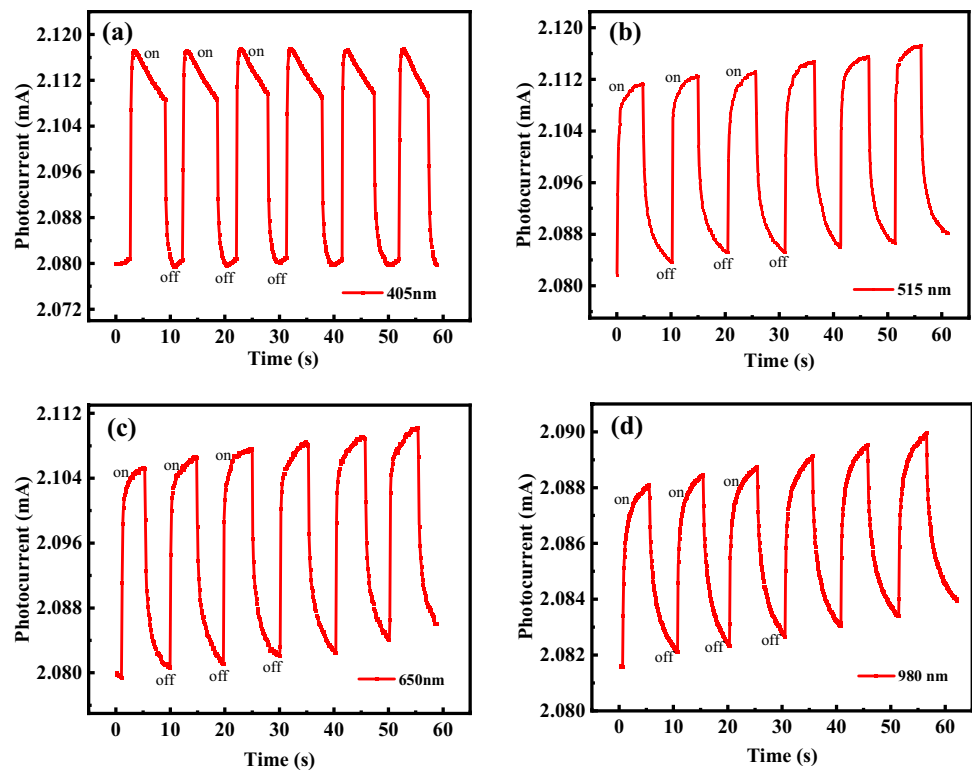
Fig. 5 a The photocurrent spectrum of the graphene/PbS hybrid photodetector. **b** Responsivity and detectivity as a function of four different wavelengths of 0.16 mW/cm²

incident wavelengths, which is in agreement with the optical absorption spectra of the PbS QDs thin films.

The responsivity (R) and detectivity (D^*) are calculated by the following formula [22]:

$$R = \frac{I_{ph}}{P_i S},\qquad(1)$$

$$D^* = \frac{R\sqrt{A}}{\sqrt{2qI_{dark}}},\qquad(2)$$

where I_{ph} is the photocurrent, P_i is the incident light irradiance, S is the active area of the phototransistor, A is the active area of illumination, q is the electron charge and I_{dark} is the dark current. By calculation, the R and D^* of the hybrid photodetector are 7.7×10^2 A·W⁻¹ (8.93×10^9 Jones), 6.4×10^2 A·W⁻¹ (7.44×10^9 Jones), 5.4×10^2 A·W⁻¹ (6.27×10^9 Jones) and 2×10^2 A·W⁻¹ (2.32×10^9 Jones) at the 405 nm, 515 nm, 650 nm and 980 nm, respectively. The variation curve of responsivity with different wavelengths is shown in Fig. 5b. The results signify the high photoresponsivity and detectivity of the hybrid photodetector in the whole tested wavelength range. In particular, the maximum R of 7.7×10^2 A·W⁻¹ is achieved under 405 nm laser illumination. This value is much higher than those reported in the literature based on pure monolayer graphene photodetectors [23].

Also, the external quantum efficiency (*EQE*) is defined as $(1.24 \times R)/\lambda$, where *R* is the photoresponsivity and λ is the incident light wavelength. The value of *EQE* is $2.53 \times 10^2 \%$ at 980 nm. The high *R* and *EQE* can be attributed to photoconductive gain (*G*) which is determined by the ratio of the lifetime of carriers (τ) and transit time (τ_t).

The carrier mobility (μ) can be obtained from the transfer characteristic according to the formula [24]:

$$\mu = \frac{L}{WC_{ox}V_{ds}} \frac{\partial I_D}{\partial V_{gs}}, \qquad (3)$$

where *W* and *L* are the width and length of the channel, respectively. C_{ox} is the capacitance per unit area of the gate medium. Here, $W = 3000$ μm, $L = 30$ μm, $V_{ds} = 0.2$ V, $C_{ox} \sim 3$ fF/μm^2, and $(\partial I_{ds}/\partial V_{gs})_{max} = 0.8$ mA/V, which is calculated by fitting Fig. 3b, we calculate the carrier mobility $\mu = 1600$ cm^2/V·s. The transit time of $L = 30$ μm long device from Fig. 1b is about 28 ns ($\tau_t = L^2/(\mu \cdot V_{ds})$) [22]. This results in a gain of 3×10^7, considering the lifetime (τ) of about 1 s. This gain value is higher than photodetectors with transition metal dichalcogenides hybrid structures ($\sim 3 \times 10^4$), and carbon nanotube structures ($\sim 10^5$) [25, 26].

To test the stability of the hybrid photodetector under light illumination, we deliberately increased the on/off period (> 25 cycles) when measuring the response of the device to the laser at wavelengths 405 nm, 515 nm, and 650 nm. The results are shown in Fig. 6. Obviously, the device can maintain a stable photoresponse for more than 250 s at least when the laser is periodically switched on and off 25 times, and the photocurrent of each cycle remains consistent, indicating that the device has excellent reproducibility and stability. Also, it should be pointed out that, although the device has an obvious response to the illumination of the 980 nm laser source, the photocurrent
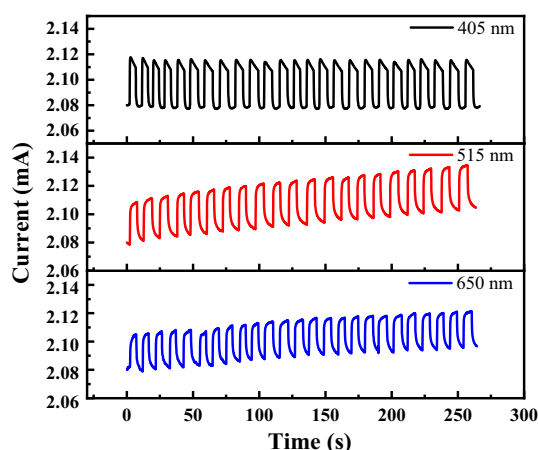
sharply will decrease after about ten periods due to the strong thermal effect of the 980 nm laser. We are considering and trying an effective way to reduce the thermal effect and improve the response performance of the device under infrared laser illumination.

Lastly, a nonnegligible phenomenon can be found that the saturation source–drain current of the device is gradually increasing. From Fig. 6, the maximum source–drain current of the device with 515 and 650 nm laser illumination increases with the increase of illumination time, but the maximum source–drain current of the device with 405 nm laser illumination gradually stabilizes over time and tends to be stable. We think the gradual increase of the saturation source–drain current of the device may be caused by the capacitance effect [27]. It can be deduced that the capacitance effect is likely to occur during the initial migration of the carriers from the channel to the source and drain electrodes. Therefore, when the time-dependent photocurrent of the device was measured, the charge released by the capacitance effect will increase the source–drain current, resulting in the gradual rise of the rectangular pulse. Then in the subsequent photoresponse measurements, the optical switching characteristics of the device were restored as the disappearance of the capacitance effect.

4 Conclusion

In summary, a high-performance graphene–PbS QDs hybrid photodetector with broadband response and long-time stability was demonstrated in detail. The results show that the hybrid photodetector has an obvious response to illumination laser from 405 to 980 nm, exhibiting excellent broadband photoresponse performance. The maximum photoresponsivity of this device is 7.7×10^2 A·W^{-1} (8.93×10^9 Jones), under the 405 nm laser illumination, and the photoconductive gain is 3×10^7. The hybrid photodetector can also maintain stable photoresponse for more than 250 s and 25 on/off switching cycles at least, indicating the excellent reproducibility and stability of the device.

Author contributions Jiajin Zheng wrote the main manuscript text; Wanchao Di, BeiBei Bao, and Jiaqi Lu performed the experiment; kehan Yu and Wei Wei contributed significantly to analysis and manuscript preparation;

Fig. 6 Long-time response with more than 250 s of three different wavelengths

Declarations

Competing interests The authors declare no competing interests.

References

1. Q. Ma, C.H. Lui, J.C.W. Song, Y. Lin, J.F. Kong, Y. Cao, T.H. Dinh, N.L. Nair, W. Fang, K. Watanabe, Giant intrinsic photoresponse in pristine graphene. Nat. Nanotechnol. **14**(2), 145–150 (2019)
2. D.J. Akinwande, C. Huyghebaert, C.H. Wang, M.I. Serna, S. Goossens, L.J. Li, H.S.P. Wong, F.H.L. Koppens, Graphene and two-dimensional materials for silicon technology. Nature **573**(7775), 507–518 (2019)
3. J. Han, M. He, M. Yang, Q. Han, F. Wang, F. Zhong, M. Xu, Q. Li, H. Zhu, C. Shan, Light-modulated vertical heterojunction phototransistors with distinct logical photocurrents. Light Sci. Appl. **9**(1), 1–10 (2020)
4. A.K. Geim, K.S. Novoselov, The rise of graphene. Nat. Mater. **6**(3), 183–191 (2007)
5. J.Y. Moon, M. Kim, S.I. Kim, S. Xu, J.H. Lee, Layer-engineered large-area exfoliation of graphene. Sci. Adv. **6**(44), 6601 (2020)
6. A. Shultz, Bo. Liu, M. Gong, M. Alamri, M. Walsh, R.C. Schmitz, J.Z. Wu, Development of broadband PbS quantum dot/graphene photodetector arrays with high-speed readout circuits for flexible imagers. ACS Appl. Nano Mater. **5**(11), 16896–16905 (2022)
7. S. Chugh, R. Mehta, Lu. Ning, F.D. Dios, M.J. Kim, Z. Chen, Comparison of graphene growth on arbitrary non-catalytic substrates using low-temperature PECVD. Carbon **93**, 393–399 (2015)
8. P.D. Kaushik, M. Rodner, G.B.V.S. Lakshmi, I.G. Ivanov, G. Greczynski, J. Palisaitis, J. Eriksson, P. Solanki, A. Aziz, A.M. Siddiqui, R. Yakimova, G.R. Yazdi, Surface functionalization of epitaxial graphene using ion implantation for sensing and optical applications. Carbon **157**, 169–184 (2020)
9. M. Freitag, T. Low, P. Avouris, Increased responsivity of suspended Graphene photodetectors. Nano Lett. **13**(4), 1644–1648 (2013)
10. E.O. Polat, O. Balci, N. Kakenov, H.B. Uzlu, C. Kocabas, R. Dahiya, Synthesis of large area graphene for high performance in flexible optoelectronic devices. Sci. Rep. **5**, 16744 (2015)
11. Y.Q. Huang, R.J. Zhu, N. Kang, J. Du, Photoelectrical response of hybrid graphene-PbS quantum dot devices. Appl. Phys. Lett. **103**(14), 666 (2013)
12. S. Bansal, K. Prakash, K. Sharma, N. Sardana, A.K. Singh, A highly efficient bilayer graphene/ZnO/silicon nanowire-based heterojunction photodetector with broadband spectral response. Nat. Nanotechnol. **31**(40), 405205–405215 (2020)
13. C.O. Kim, S. Kim, D.H. Shin, S.S. Kang, J.M. Kim, C.W. Jang, S.S. Joo, J.S. Lee, J.H. Kim, S.H. Choi, High photoresponsivity in an all-graphene p-n vertical junction photodetector. Nat. Commun. **5**, 3249 (2014)
14. J. Zhang, R.W. Crisp, J. Gao, D.M. Kroupa, M.C. Beard, J.M. Luther, Synthetic conditions for high-accuracy size control of pbs quantum dots. J. Phys. Chem. Lett. **6**(10), 1830–1833 (2015)
15. I. Moreels, Y. Justo, B.D. Geyter, K. Haustraete, J.C. Martins, Z. Hens, Size-tunable, bright, and stable PbS quantum dots: a surface chemistry study. ACS Nano **5**(3), 2004–2012 (2011)
16. R.D. Harris, S.B. Homan, M. Kodaimati, H. Chen, E.A. Weiss, Electronic processes within quantum dot-molecule complexes. Chem. Rev. **116**(21), 12865–12919 (2016)
17. C.R. Kagan, E. Lifshitz, E.H. Sargent, D.V. Talapin, Building devices from colloidal quantum dots. Science **353**(6302), 5523 (2016)
18. H. Jeong, J.H. Song, S. Jeong, W.S. Chang, Graphene/PbS quantum dot hybrid structure for application in near-infrared photodetectors. Sci. Rep. **10**(1), 12475 (2020)
19. Z. Ren, J. Sun, H. Li, P. Mao, Y. Wei, X. Zhong, J. Hu, S. Yang, J. Wang, Bilayer PbS quantum dots for high-performance photodetectors. Adv. Mater. **29**(33), 1702055 (2017)
20. I. Zheng, X. Xu, Y. Zhang, Q. Xie, W. Wei, Photodetectors based on controllable growth of large-area graphene films. Thin Solid Films **709**, 138129 (2020)
21. Z.H. Sun, Z.K. Liu, J.H. Li, G.A. Tai, S.P. Lau, F. Yan, Infrared photodetectors based on CVD-grown graphene and PbS quantum dots with ultrahigh responsivity. Adv. Mater. **24**(43), 5878–5883 (2012)
22. S. Lee, J. Park, Y. Yun, J. Lee, J. Heo, Enhanced photoresponsivity of multilayer mos2 phototransistor using localized Au Schottky junction formed by spherical-lens photolithography. Adv. Mater. Interfaces **6**(8), 1053 (2019)
23. R.C. Guo, W.H. Liu, Y.T. Zhang, Z.Q. Hou, C. He, H. Li, Multichannels electrode parallel structure graphene photodetector with high performance. Mater. Lett. **260**, 126948 (2019)
24. G. Konstantatos, M. Badioli, L. Gaudreau, J. Osmond, M. Bernechea, P.G.D. Arquer, F. Gatti, F.H.L. Koppens, Hybrid graphene-quantum dot phototransistors with ultrahigh gain. Nat. Nanotechnol. **7**(6), 363–368 (2012)
25. H.J. Tan, W.S. Xu, Y.W. Sheng, C.S. Lau, Y. Fan, Q. Chen, M. Tweedie, X.C. Wang, Y.Q. Zhou, J.H. Warner, Lateral graphene-contacted vertically stacked WS2/MoS2 hybrid photodetectors with large gain. Adv. Mater. **29**(46), 1702917–1702925 (2017)
26. Y.D. Liu, F.Q. Wang, X.M. Wang, X.Z. Wang, E. Flahaut, X.L. Liu, Y. Li, X.R. Wang, Y.B. Xu, Y. Shi, R. Zhang, Planar carbon nanotube-graphene hybrid films for high-performance broadband photodetectors. Nat. Commun. **6**, 8589 (2015)
27. T.B. Adams, D.C. Sinclair, A.R. West, Giant Barrier layer capacitance effects in $CaCu_3Ti_4O_{12}$ ceramics. Adv. Mater. **14**(18), 1321–1323 (2002)